

# Nanomachining of multilayer graphene using an atomic force microscope

P. Barthold, T. Lüdtkke, and R. J. Haug

*Institut für Festkörperphysik, Leibniz Universität Hannover, Appelstr. 2, 30167 Hannover, Germany*

(Dated: November 16, 2018)

An atomic force microscope is used to structure a film of multilayer graphene. The resistance of the sample was measured *in-situ* during nanomachining a narrow trench. We found a reversible behavior in the electrical resistance which we attribute to the movement of dislocations. After several attempts also permanent changes are observed. Two theoretical approaches are presented to approximate the measured resistance.

PACS numbers: 73.63.-b, 73.23.-b, 81.07.-b, 81.16.-c

Atomic force microscopes (AFMs) are well known tools for imaging and for structuring. Besides other lithographic methods nanomachining with the AFM is a simple, but highly efficient way to design devices on the sub-micron level. By applying a high contact force between sample and AFM tip a permanent deformation of the sample's surface is obtained. Using this method different materials have been structured e.g. semiconductors [1, 2, 3] and metals [4].

Up to now the common technique to structure graphene is by etching. [5, 6, 7] Graphene has drawn a great deal of attention since the discovery of free standing single layer graphite (so-called graphene) and its unique electronic properties. [8, 9, 10, 11] The motivation for the work presented here was to structure graphene via nanomachining with an AFM tip. We structured a thin film of graphite by nanomachining a trench through the half width of the sample. Hence the conducting area of the sample is reduced and thereby a constriction is formed. Thereby we observed an interesting reversible behavior in the resistance and in the end a permanent change in the resistance.

The graphite sample used in this study is extracted from natural graphite [12] by exfoliation [13] on a silicon substrate with a 300 nm SiO<sub>2</sub> layer. The thereby formed flake has a lateral dimension of a few micrometers and a thickness of about 10 nm ( $\sim 30$  atomic layers, assuming a lattice constant of 0.34 nm). The Ti/Au (9 nm/46 nm) electrodes are fabricated using standard electron beam lithography. After bonding the sample it is electrically contacted inside the AFM allowing *in-situ* measurements at room temperature. Figure 1 shows the general setup. A direct current of  $I = 500$  nA is driven via two contacts through the sample while the voltage  $V$  is measured using the two remaining electrodes. For the measurements presented here we used an AFM tip that is coated with polycrystalline diamond on the tip-side. During the measurements we applied a force of approximately  $0.5 \mu\text{N}$ . Using such a high contact force the tip is moved with a velocity of about  $0.5 \mu\text{m/s}$  half the way across the graphite flake as sketched by the white arrows in Fig. 1. The tip starts its movement left of the flake, moves about  $2.2 \mu\text{m}$  through the flake and returns back to its starting position. Thus the tip scratches the sample in both directions. After five of those movements a distinct trench

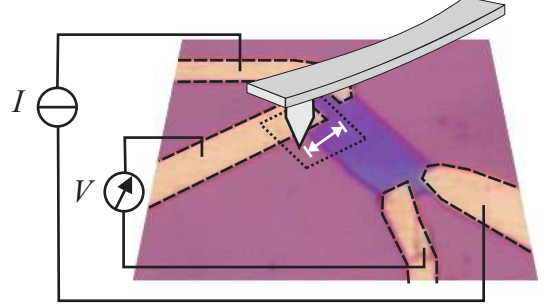


FIG. 1: Schematic drawing of the setup. The optical picture shows the graphite flake with four electrodes. A direct current is driven through the sample via two contacts while the voltage is measured using the other two electrodes. The AFM tip moves from left to right and to the left again while a high contact force is applied. The dashed square marks the region which is shown in Fig. 2(a) and (b).

is formed in the graphite film.

Figures 2(a) and (b) show two AFM pictures of the sample before and after nanomachining. A trench of about  $2.2 \mu\text{m}$  is clearly visible in the graphite flake in Fig. 2(b). Figure 2(c) demonstrates the time evolution of the overall resistance  $R$  while scratching the graphite film with the AFM tip. To demonstrate the resistance change of the structured part  $\Delta R_S$  is shown in Fig. 2(d). The time period when the tip moves on top of the graphite is marked grey in Fig. 2(c) and (d). At  $t = 0$  s the resistance of the sample is about  $R \approx 248 \Omega$  ( $\Delta R_S = 0 \Omega$ ). At  $t \approx 15$  s when the tip is moved over the graphite for the first time (I) with the high contact force the resistance starts to increase. The resistance reaches its first maximum of  $R \approx 258 \Omega$  ( $\Delta R_S \approx 15 \Omega$ ) at  $t \approx 21$  s which coincides with the reversal point of the AFM tip movement. The resistance drops again to its original value by moving the tip back to the original starting position. When the tip applies a force to the graphite for the second time the resistance starts to rise again (II). This time the value rises up to about  $275 \Omega$ . Afterwards the resistance drops to a value of  $248 \Omega$  ( $\Delta R_S = 0 \Omega$ ). As the AFM tip moves over the flake for the third time (III) the resistance in-

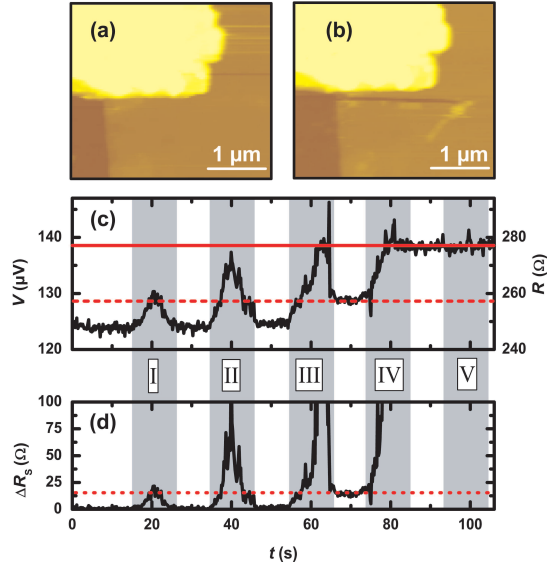


FIG. 2: Upper part: AFM images of the graphite flake with a height of about 10 nm. (a) Magnification of the interesting part as marked in Fig 1. (b) After nanomachining five times with the AFM tip. A clear trench in the graphite is visible. Its dimensions are  $w_S \approx 2.2 \mu\text{m}$  and  $l_S \approx 100 \text{ nm}$ . (c) Time evolution of the resistance of the sample while the AFM tip applies a force to the graphite. The grey regions indicate when the tip actually moves on top of the graphite, the roman numerals count the number of movements. The dashed and solid vertical lines are guides to the eye to stress the similar resistances of the sample during different times of structuring. (d) The resistance change of the structured part  $\Delta R_S$  is shown.  $\Delta R_S$  is extracted from Fig. 2(c) by subtracting  $R(t = 0 \text{ s})$  leading to  $\Delta R_S = 0 \Omega$  and putting  $\Delta R_S(t = 500 \text{ s})$  to infinity as the graphite is cut through in this part of the sample.

creases to a value of about  $277 \Omega$ . Now the resistance decreases to  $R \approx 258 \Omega$ , which is  $10 \Omega$  higher than the overall resistance in the beginning and corresponds to a  $\Delta R_S \approx 15 \Omega$ . The value after the third tip movement is the same as the maximum obtained during AFM run I, as indicated by the dashed line in Fig. 2(c). As the tip moves for the fourth time (IV) over the graphite, the resistance rises again to a value of about  $277 \Omega$ . The same value is already reached during run II and III. But this time the resistance does not drop again instead it stays at a value of  $R \approx 277 \Omega$ . This resistance is kept even when the tip moves for a fifth time (V) on top of the graphite and stays at this value afterwards. Thus the resistance of the graphite film was permanently changed by  $29 \Omega$  using an AFM tip to structure it.

To explain this behavior we consider the following model: While the AFM tip is moved over the sample dislocations are induced along the trajectory of the movement of the tip as schematically depicted in Fig. 3(b). These dislocations modify the electronic properties of the sample. Thus the resistance of the sample rises during scratching. These dislocations then move to the edge of the sample where we assume that their influence on the

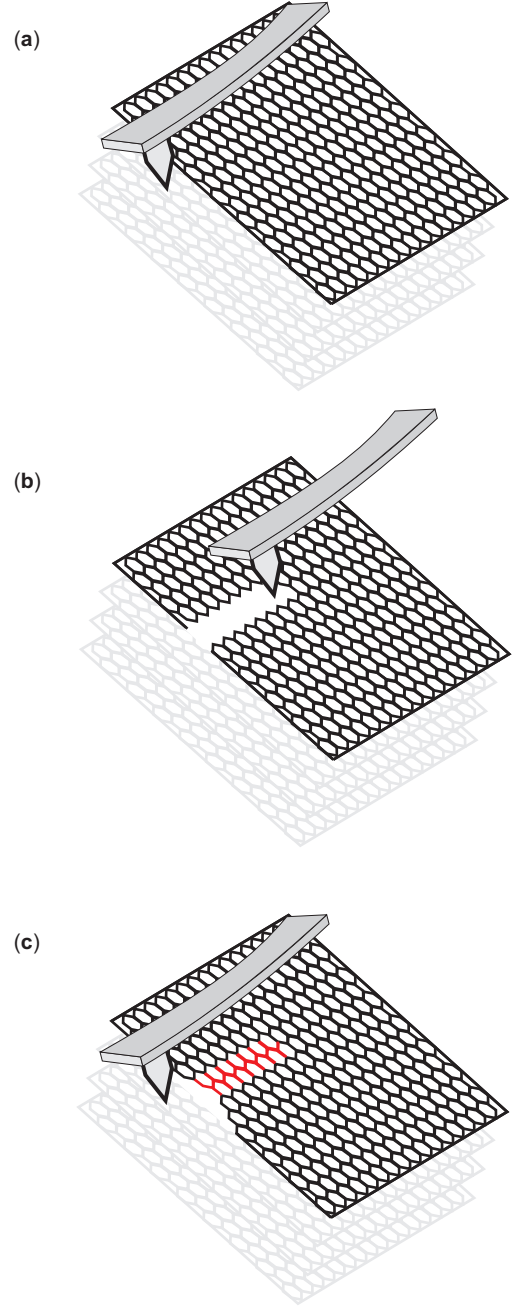


FIG. 3: A simplified schematic sketch of the AFM tip as the graphene layers are nanomachined. (a) The sample is still unperturbed. (b) The tip has been moved over the sample and bonds have been destroyed. (c) as the tip moves back the induced dislocations start to move to the edge of the sample.

electronic properties of the flake is only small illustrated in Fig. 3(c). Grenall reported dislocation movement in smeared flakes of natural graphite. [14] As observed by Williamson dislocations in graphite run parallel to the layer plane. [15] Mainly they move to the edge of the flake or to cleavage steps. Hence bonds just destroyed by the AFM tip along the trajectory of the movement could close again and the transport properties get back

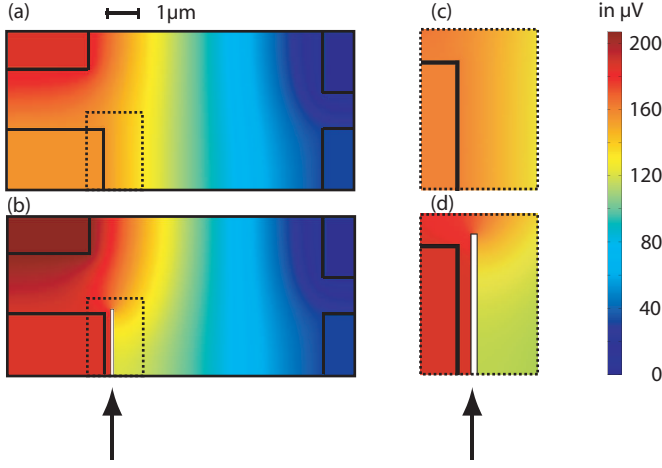


FIG. 4: Top view of the numerical calculated electrical potential of the sample. The arrow marks the nanomachined trench. The gold electrodes are depicted by the black rectangles on the edges of the sample. The current is driven through the upper contacts while the lower ones are used to measure the voltage drop. (a) The electrical potential drop of the unperturbed sample. (b) Sample after five runs with the AFM and a trench formed with the dimensions  $w_S \approx 2.2 \mu\text{m}$  and  $l_S \approx 100 \text{ nm}$ . A dramatic change in the potential drop between the two lower electrodes is clearly visible, (c) shows a magnification of the later structured part and (d) demonstrates a blow up of the surrounding of trench.

to the original state, thus the resistance drops again to its original value.

As our sample consists of many layers, it seems reasonable to believe that during the first time the sample is scratched (I) dislocations are induced only in the few upper layers and during the second time (II) dislocations are induced in more layers. This would explain the higher resistance during run II compared to I. As the resistance during run II is close to the value reached at the end, dislocations seem to be formed in most of the layers when scratching for the second time.

The defects induced during the second time of scratching could move again to the edge of the sample. Therefore the resistance drops (between II and III) to its original value. During the third time of scratching (III) a lasting deformation occurs for the first time. In a few layers the bonds destroyed by the AFM tip are not closed again and thereby influence the electronic properties of the sample permanently. During the fourth run (IV) all layers are cut through on a  $2.2 \mu\text{m}$  long path along the sample. Thus the resistance keeps its value even when it is scratched for the fifth time. All bonds are destroyed along the trajectory of the movement of the AFM tip.

What follows now are two theoretical approaches to get an understanding of the nanomachining process in terms of the measured resistances. In a first step to model the resistances we start with Ohm's law:

$$\mathbf{J} = \sigma \mathbf{E}, \quad (1)$$

where  $\mathbf{J}$  is the current density,  $\sigma = \rho^{-1}$  the conductivity tensor,  $\mathbf{E} = -\nabla V$  is the electric field with the potential  $V$ . Applying the conservation of currents to Eq. 1 leads to:

$$\nabla \mathbf{J} = \nabla \sigma \mathbf{E} = -\nabla \cdot (\sigma \nabla V) = 0 \quad (2)$$

The current is driven through the upper left electrode in Fig. 4. The boundary conditions were selected to be electrically insulating (the normal component of the current density is zero,  $\mathbf{n} \cdot \mathbf{J} = 0$ ). The second order partial differential Eq. 2 is numerically solved. The calculations were performed using finite elements within in a mesh of around 40,000 elements.[18] This is a three dimensional, diffusive model. Knowing the geometry of the sample we find a sheet resistivity of  $\rho \approx 2.03 \cdot 10^{-6} \Omega\text{m}$ . The measured values are  $R \approx 248 \Omega$ ,  $l \approx 7.3 \mu\text{m}$ ,  $w \approx 5.2 \mu\text{m}$ , and  $h \approx 10 \text{ nm}$ , where  $l$  is the length in current direction,  $w$  the width orthogonal to the current direction, and  $h$  the height of the sample. By applying these values to the textbook formula  $\rho = R \cdot w \cdot h / l$ , the resulting resistivity is  $\rho \approx 1.77 \cdot 10^{-6} \Omega\text{m}$ , being comparable to the one found by our numerical calculations and the specific resistance  $\rho \approx 1.2 \cdot 10^{-6} \Omega\text{m}$  reported by Powell et al. for natural graphite. [17] The reason for the difference between these two latter results might be that the resistivity of graphite depends strongly on the doping of the sample and thereby varies from sample to sample and Powell et al. report the specific resistances of samples that are in the dimensions of a few millimeters and centimeters. The difference compared to the numerical calculations is caused by the fact that the textbook formula describes an ideal macroscopic system. In the numerical model for our mesoscopic device the asymmetry in the electrodes of our sample is taken into account. Therefore we will use  $\rho \approx 2.03 \cdot 10^{-6} \Omega\text{m}$  for our further calculations.

Figure 4 shows the results of the numerical simulation. The electrical potential of the intact flake Fig. 4 (a) and the potential of the sample in the end with the formed trench Fig. 4 (b) are compared. If a trench with  $w_S = 2.2 \mu\text{m}$  and  $l_S = 100 \text{ nm}$  is simulated within this numerical model a drastic change in the electrical potential is clearly visible. Figure 4 (c) and (d) illustrate the dramatic influence of the relatively small trench on the electrical potential of the sample. This radical change in the potential leads to a resistance change between the lower electrodes in Fig. 4 of  $63 \Omega$  (measured resistance change  $29 \Omega$ ). As we are dealing here with a mesoscopic device, reasons for the differences between the measured and the calculated resistance change might be that neither side-effects nor quantum effects are taken into account by the simulation. In addition the nanomachined trench is relatively small compared to the size of the sample. The numerical model simulates the whole sample and as it provides good results for the global measured effects, we consider another theoretical approach that describes the resistance change from a more local point of view.

For this we compare our results to findings of García et

al. [19] who used an exact evaluation of Maxwell's solutions for a spreading, ohmic resistance of a constriction separating two semi-infinite media. In this two dimensional model the resistance value contributed by the formed trench in the end can be described using Eq. 4 from [19], which could be written in the following form for our problem:

$$R_{2d} = \frac{2a\rho}{h\pi} \cdot \ln\left(\frac{w}{w - w_s}\right), \quad (3)$$

where  $R_{2d}$  is the spreading, ohmic resistance of the constriction,  $a$  is a constant that takes care of the influence of the sample shape and the topology of the electrodes position, and  $w$  is the width of the sample, whereas  $w_s$  is the width of the structured part, hence  $w - w_s$  is the width of the constriction. As we are at room temperature ballistic parts are negligible. Also the length of the constriction is much smaller than the width, and therefore it also does not contribute. In our device the most of the voltage drop measured by the electrodes is given by the  $7.3 \mu\text{m}$  long path, therefore the increase in the resistance due to the constriction can be estimated by using Eq. 3. With  $\rho = 2.03 \cdot 10^{-6} \Omega\text{m}$ ,  $h = 10 \text{ nm}$ ,  $w = 5.2 \mu\text{m}$ ,  $w - w_s = 3 \mu\text{m}$  and  $a = 1/2$  it leads to  $R_{2d} \approx 35.5 \Omega$ . With  $R \approx 248 \Omega$  of the unperturbed sample this results in  $R = 283.5 \Omega$  in the end, which compares nicely with our measured resistance  $R \approx 277 \Omega$ . As this model only describes the resistance change due to the locally formed constriction, it is not dependent on the geometry and homogeneity of the rest of the sample. Therefore it is quite reasonable that this estimation fits better than the numerical evaluation which depends on the whole sample. In a perfectly shaped and homogeneous device both results should converge to one another. Let us point out

that both here used methods to estimate the quantitative findings are rough assumptions, based on the one hand side on a three dimensional, numerical model and on the other hand side on a strictly two dimensional, analytical approach. An adequate model to describe our device in more detail would be needed.

In conclusion, we have shown *in-situ* measurements of the resistance of mesoscopic graphite being nanomachined with a diamond coated AFM tip, for one exemplary sample, other measured results can be found in Ref. [20]. During processing the device we find a reversible change in the electrical resistance. We attribute this effect to induced dislocations that lead to an increased resistance. At room temperature these dislocations can easily move to the edges of the graphite flake leading to reversible resistance changes. After processing the sample with the AFM tip a couple of times the resistance changes permanently, i.e. bonds inside the graphite are broken permanently. Two different theoretical models are demonstrated to estimate the measured resistance changes. Further investigations of the reversible resistance change should be performed varying other parameters as for example the temperature and the velocity of the AFM tip movement to see how the reversing of the resistance depends on those parameters and to learn more about the influence of the dislocation movement on the electronic properties of graphene layers. Forming smaller constrictions the observation of ballistic contribution in the transport should be possible. [19] The here presented technique to nanomachine mesoscopic graphite with an AFM contributes to the promising prospective approach to create a device based on single layer graphene which has not yet been successful. [21]

- 
- [1] R. Magno and B. R. Bennett, Appl. Lett. Phys. **70**, 1855 (1997).
  - [2] H. W. Schumacher, U. F. Keyser, U. Zeitler, R. J. Haug, and K. Eberl, Appl. Phys. Lett. **75**, 1107 (1999).
  - [3] J. Regul, U. F. Keyser, M. Paesler, F. Hohls, U. Zeitler, R. J. Haug, A. Malavé, E. Oesterschulze, D. Reuter, and A. D. Wieck, Appl. Phys. Lett. **81**, 2023 (2002).
  - [4] B. Irmer, R. H. Blick, F. Simmel, W. Gödel, H. Lorenz, and J. P. Kotthaus, Appl. Lett. Phys. **73**, 2051 (1998).
  - [5] B. Oezylmaz, P. Jarillo-Herrero, D. Efetov, and P. Kim, Appl. Lett. Phys. **91**, 192107 (2007).
  - [6] C. Stampfer, J. Güttinger, F. Molitor, D. Graf, T. Ihn, and K. Ensslin, Appl. Phys. Lett. **92**, 012102 (2008).
  - [7] S. Russo, J. B. Oostinga, D. Wehenkel, H. B. Heersche, S. S. Sobhani, L. M. Vandersypen, and A. F. Morpurgo, Phys. Rev. B **77**, 085413 (2008).
  - [8] K. S. Novoselov, A. K. Geim, S. V. Morozov, D. Jiang, Y. Zhang, S. V. Dubonos, I. V. Grigorieva, and A. A. Firsov, Science **306**, 666 (2004).
  - [9] Y. Zhang, Y.-W. Tan, H. L. Stormer, and P. Kim, Nature **438**, 201 (2005).
  - [10] K. S. Novoselov, Z. Jiang, Y. Zhang, S. V. Morozov, H. L. Stormer, U. Zeitler, J. C. Maan, G. S. Boebinger, P. Kim, and A. K. Geim, Science **315**, 1379 (2007).
  - [11] A. K. Geim and K. S. Novoselov, Nature Materials **6**, 183 (2007).
  - [12] NGS Naturgraphit GmbH.
  - [13] K. S. Novoselov, D. Jiang, F. Schedin, T. Booth, V. V. Khotkevich, S. V. Morozov, and A. K. Geim, Proc. Natl. Acad. Sci. **102**, 10451 (2005).
  - [14] A. Grenall, Nature **182**, 448 (1958).
  - [15] G. K. Williamson, Proc. Roy. Soc. **257**, 457 (1960).
  - [16] Please find an animated schematic illustration of the induced and moving dislocations as online supporting material.
  - [17] R. L. Powell and G. E. Childs, *American Institute of Physics Handbook* (McGraw-Hill, New York, 1972), pp. 4-142 to 4-160.
  - [18] The predefined environment for the dc-conductive media static case of the commercial finite elements software COMSOL has been used to solve this partial differential equation.
  - [19] N. García, P. Esquinazi, J. Barzola-Quiquia, B. Ming, and D. Spoddig, Phys. Rev. B **78**, 035413 (2008)

- [20] P. Barthold, T. Luedtke, R. J. Haug, arXiv:0803.2470v1
- [21] A. J. M. Giesbers, U. Zeitler, S. Neubeck, F. Freitag, K. S. Novoselov, and J. C. Maan, arXiv:0806.0716v2.